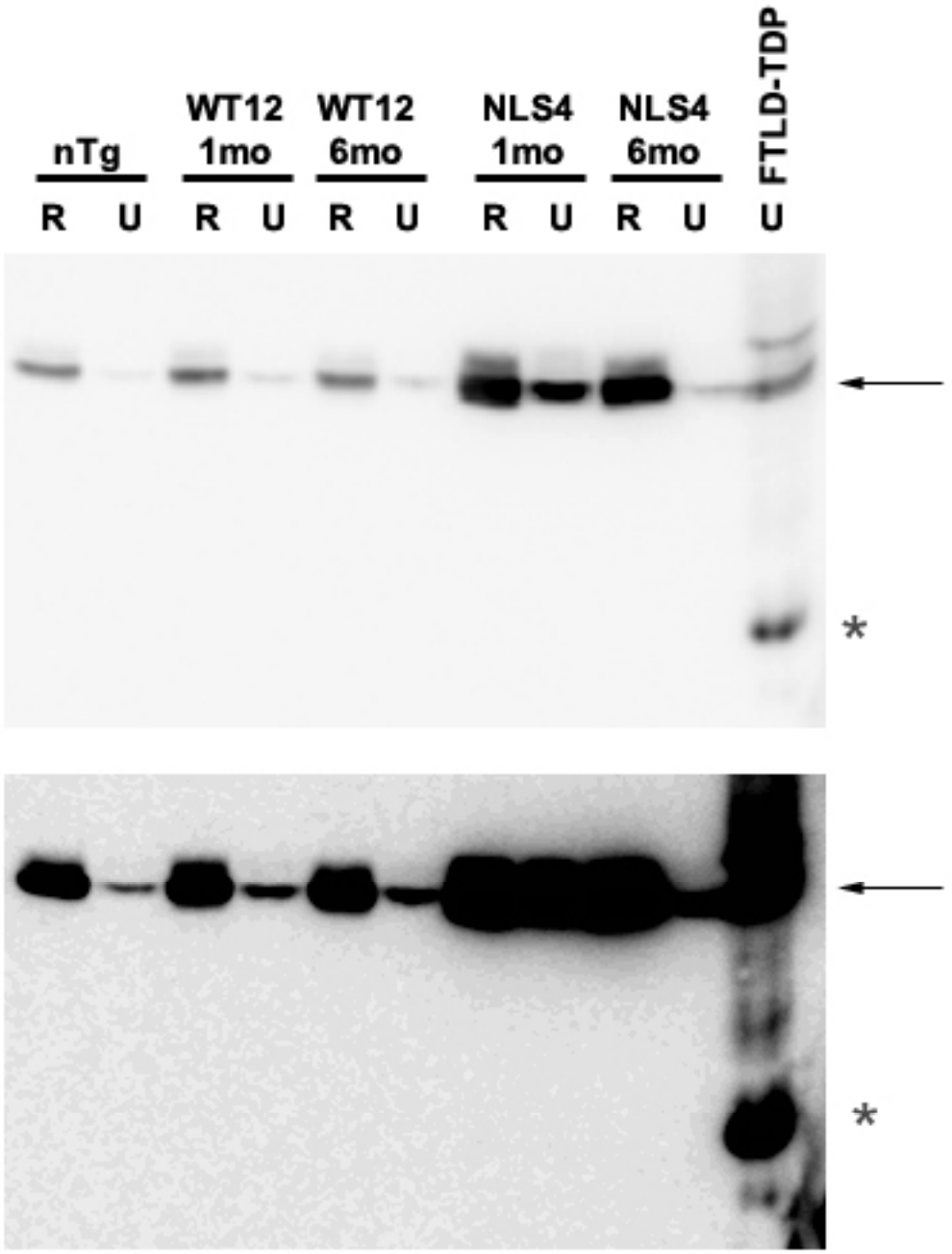

Figure S1. Absence of Detectable TDP-43 C-terminal Fragments in Tg mice. Immunoblotting for h+mTDP-43 protein of nTg, tTA/TDP-WT12 and tTA/TDP-NLS4 mice at various times off Dox was performed on RIPA and urea soluble cortical fractions. A urea soluble fraction from the neocortex of a case of FTLD-TDP is included for comparison. Light (top) and dark (bottom) exposures show full length TDP-43 protein (arrow) and no detectable C-terminal TDP-43 fragments (*).

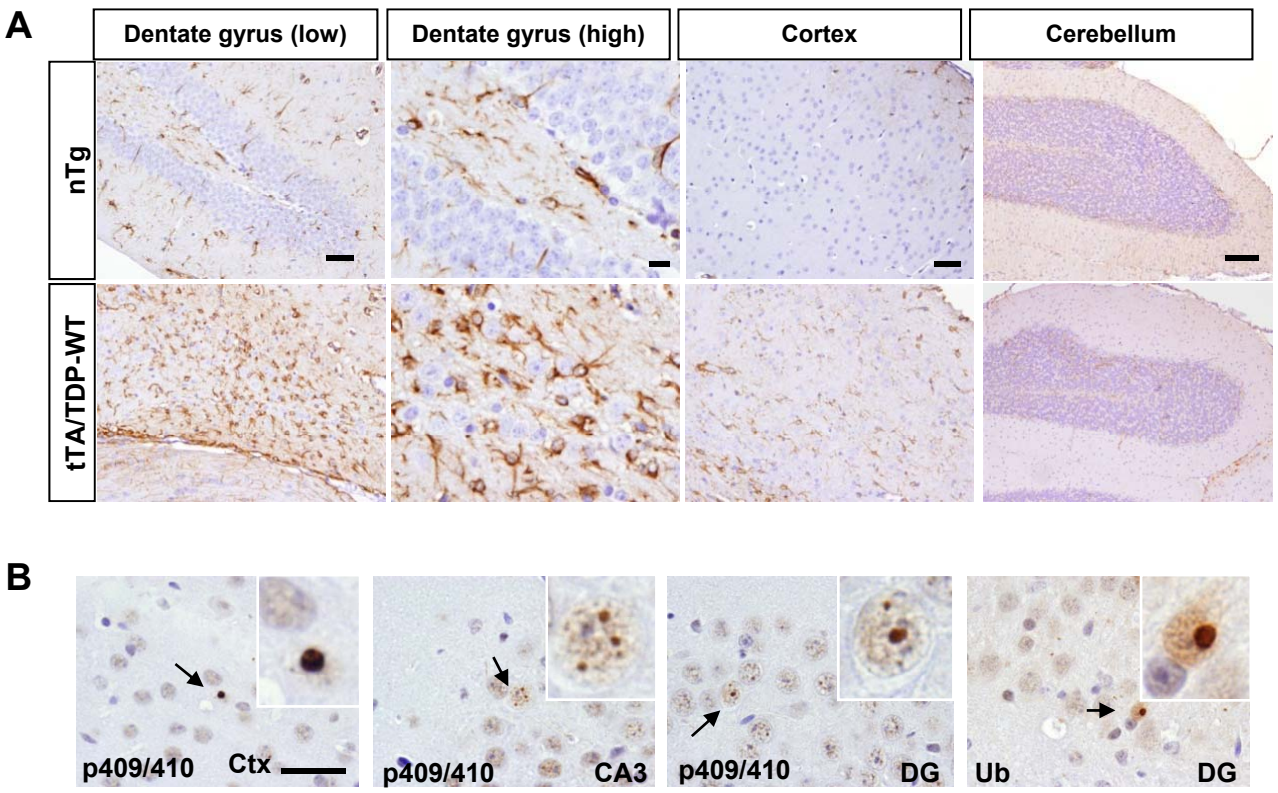

Figure S2. Gliosis and Rare Inclusions in tTA/TDP-WT Mice. (A) GFAP IHC of tTA/TDP-WT12 mice 6 months off Dox. tTA/TDP-WT mice showed reactive gliosis involving the hippocampus (low and high power images of DG are shown) and cerebral cortex corresponding to regions of high hTDP-43 expression and neurodegeneration. Hippocampus and cerebral cortex of nTg mice and cerebellum from both tTA/TDP-WT and nTg mice showed no gliosis. (B) Pathologic TDP-43 aggregates. Cortical (Ctx) or hippocampal (CA3, DG) sections from tTA/TDP-WT12 were stained for p409/410 TDP-43 and ubiquitin. Note the detection of extremely rare TDP-43 aggregates in the hippocampus and cortex. The insets display a high magnification of individual neurons (arrow) showing p409/410 TDP-43 and ubiquitin positive inclusions. Scale bars: A, 50, 10, 50 and 100 μm from left to right; B, 50 μm.

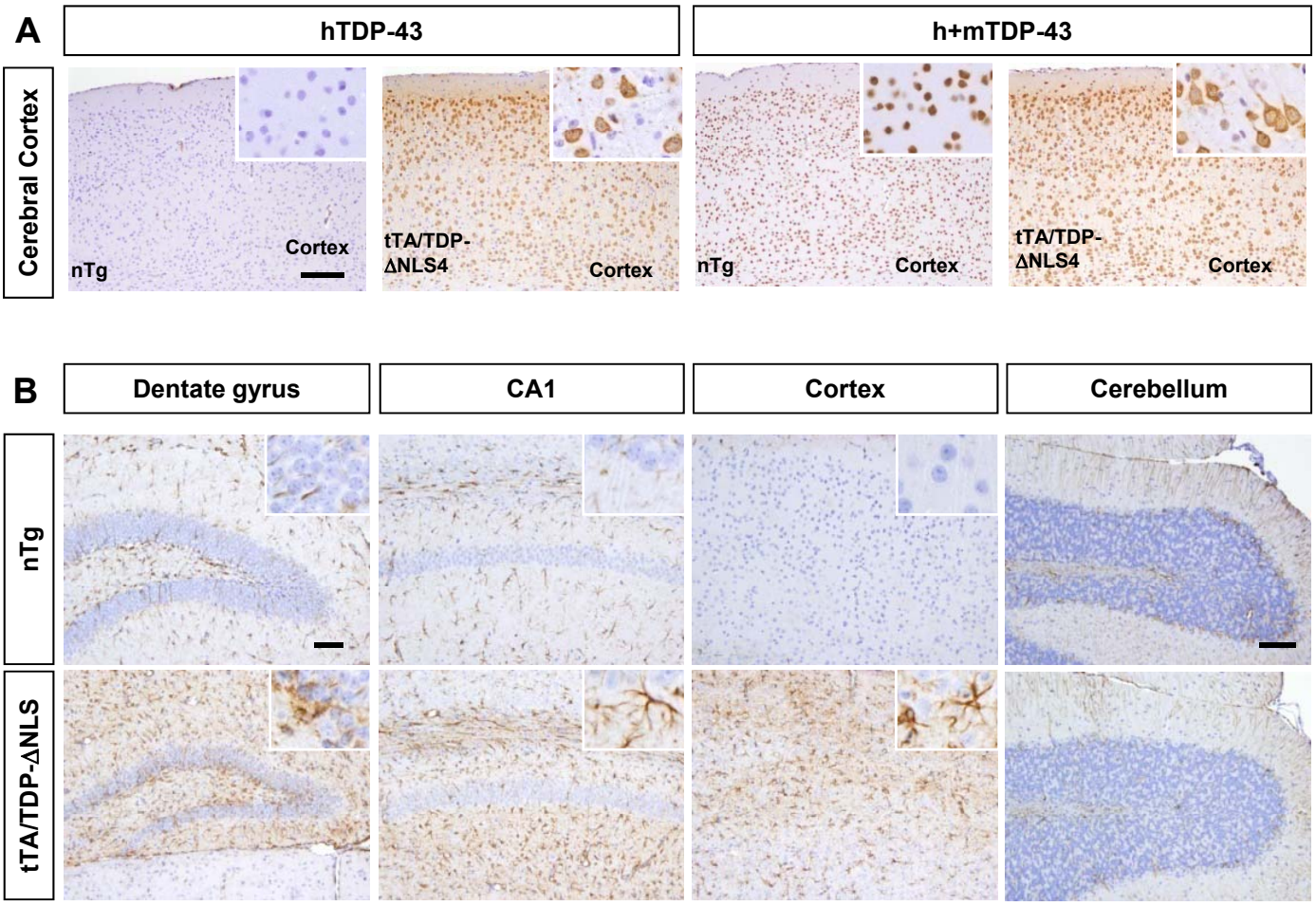

Figure S3. Cortical TDP-43 expression and gliosis in tTA/TDP-ΔNLS mice.
(A) Cytoplasmic TDP-43 expression in tTA/TDP-ΔNLS cortex. IHC for hTDP-43 (left) and h+mTDP-43 (right) show cytoplasmic TDP-43 expression in all cortical layers of tTA/TDP-ΔNLS mice in contrast with nuclear expression of h+mTDP-43 in nTg mice. Insets show higher magnification images. Scale bar 200 μm. (B) GFAP IHC of tTA/TDP-ΔNLS19 mice 1 month off Dox. tTA/TDP-ΔNLS19 mice showed reactive gliosis involving the hippocampus (Dentate gyrus, CA1 region) and cerebral cortex corresponding to regions of high hTDP-43 expression and neurodegeneration. Hippocampus and cerebral cortex of nTg mice and cerebellum from both tTA/TDP-ΔNLS and nTg mice showed no gliosis. Insets show higher magnification images. Scale bars: 50 μm for DG, CA1 and Cortex, 100 μm for cerebellum.

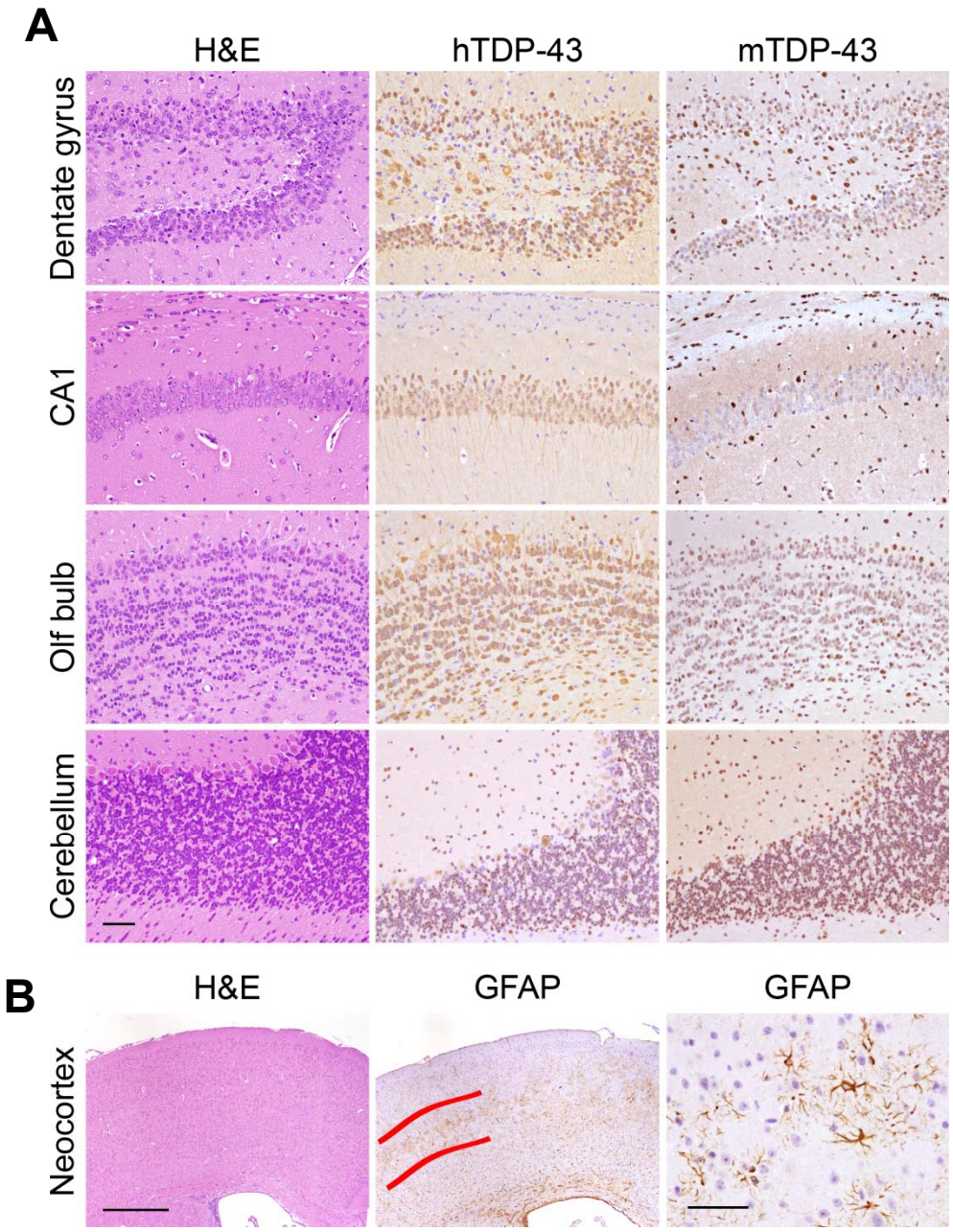

Figure S4. Selective Neuronal Vulnerability in tTA/TDP-ΔNLS Mice. (A) tTA/TDP-ΔNLS4 mice 1 mo off Dox were stained with H&E (left) and by IHC for hTDP-43 (middle) and mTDP-43 (right). Representative images of DG, hippocampal pyramidal neurons (CA1), olfactory bulb and cerebellum show selective degeneration of granular neurons of the DG while other neurons within the hippocampus and other granular cell neurons of the brain are relatively resistant. (B) H&E (left) and GFAP IHC stained sections (middle, right) of neocortex show selective gliosis of deep neocortical layers (layer V, between red lines). Scale bars: A, 50 μm; B left 500 μm, right 50 μm.

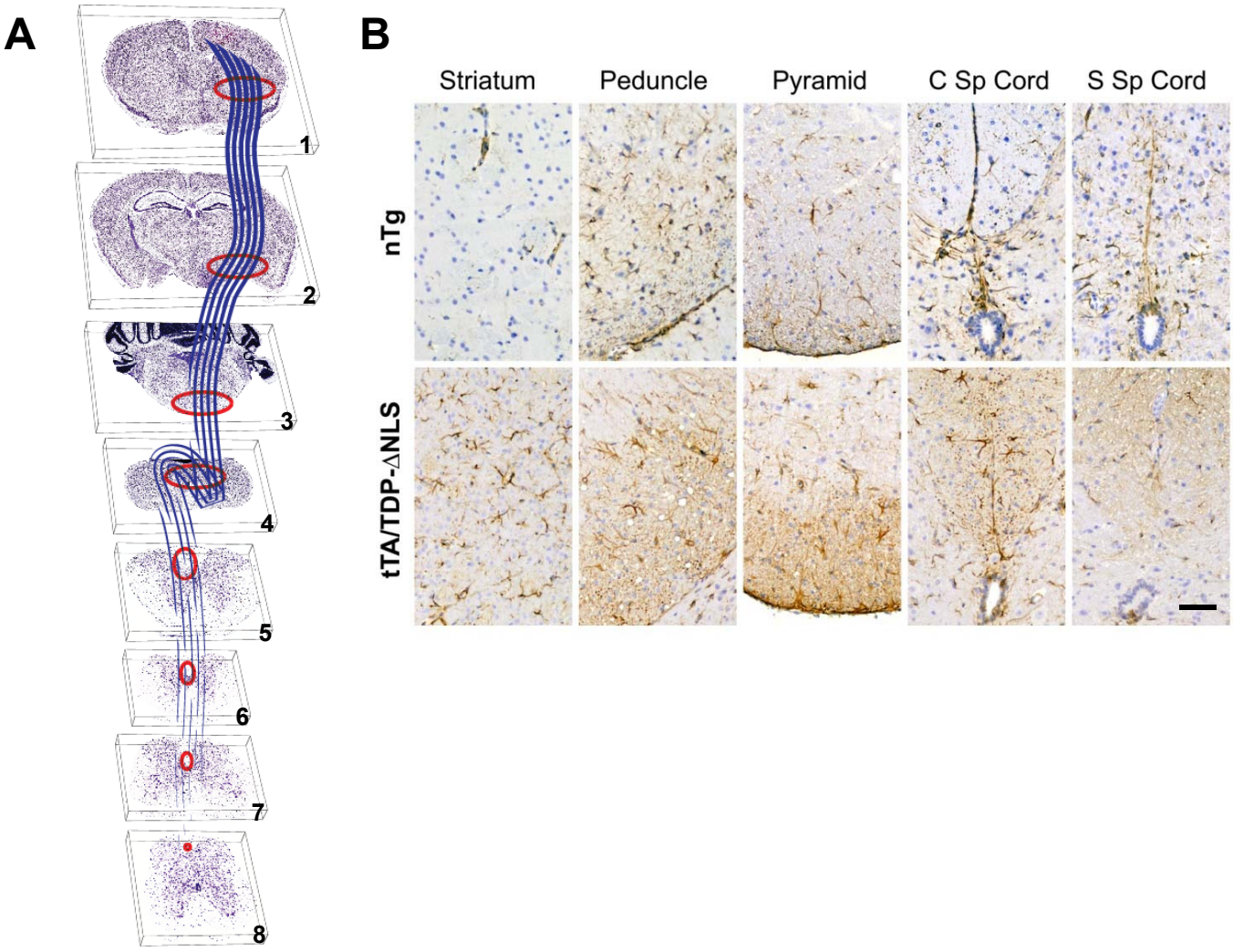

Figure S5. Gliosis of the Corticospinal Tract in tTA/TDP-ΔNLS Mice. (A) Schematic of murine corticospinal tract (CST). Motor neurons in layer V of the primary motor cortex project through the CST caudallly to the spinal cord via the internal capsule in striatum (C1), cerebral peduncles (C2) and medullary pyramids (C3) where axons decussate (C4) nearly exclusively (~95%) towards to enter the ventral portion of the dorsal columns in spinal cord (C5). As the CST (C6-8) descends caudally, there is a gradual diminution of the tract such that the CST is difficult to identify at sacral levels of the spinal cord. The derivatized images here were obtained from the Allen Mouse Brain Atlas (Seattle (WA): Allen Institute for Brain Science. http://mouse.brain-map.org). (B) Gliosis at all levels of the CST. IHC for GFAP showed reactive gliosis throughout the CST in tTA/TDP-ΔNLS4 mice one month off Dox, including the striatum, cerebral peduncles, medullary pyramids and the ventral portion of dorsal column of the cervical spinal cord (C Sp Cord). Sacral levels of the spinal cord (S Sp Cord) showed minimal gliosis of the dorsal columns, consistent with the relative absence of the corticospinal tract at these levels. Scale bar = 100 μm.

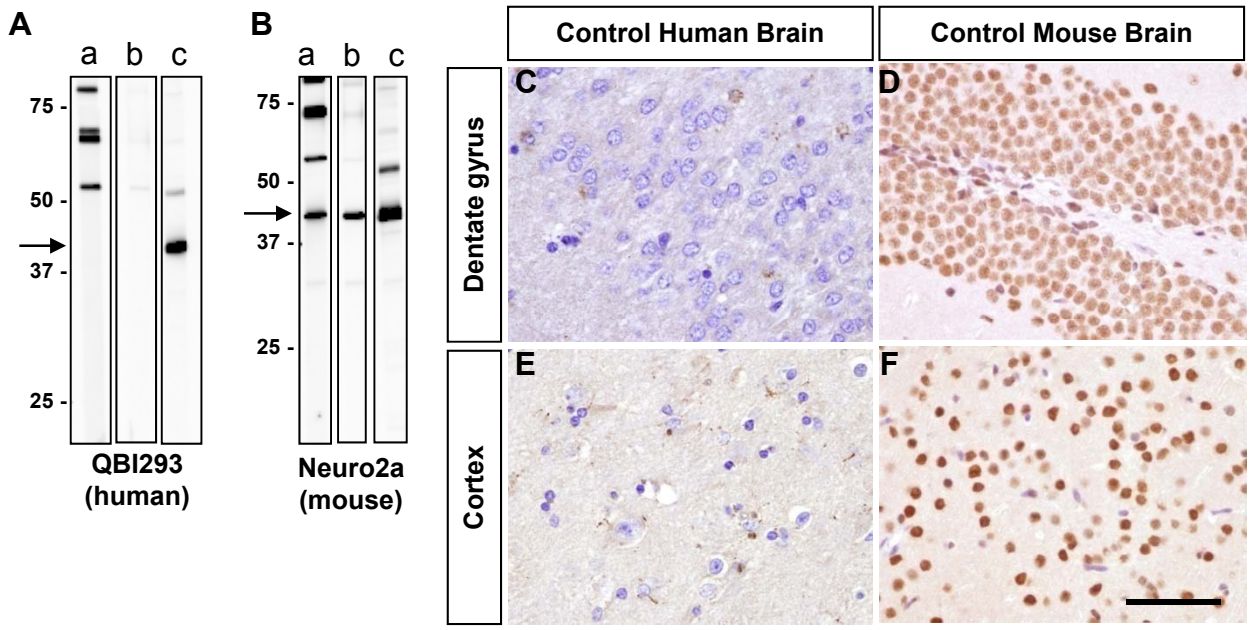

Figure S6. Generation and Characterization of a Novel Mouse-Specific TDP-43 Polyclonal Antibody.

(A-B) Immunoblotting of RIPA extracts from human QBI293 (A) or mouse Neuro2A (B) cells. An affinity-purified IgG fraction derived from antisera raised against a mTDP-43 epitope (a), a further affinity-purified fraction designated 15A using recombinant mTDP-43 (b) or a C-t h+mTDP-43 polyclonal antibody (c) were used for immunoblotting. The arrow indicates the position of the specific TDP-43 band. Note the specificity for mTDP-43 of 15A (compare b immunoblots from (A) and (B)) and the reduction of non-specific immunoreactive bands relative to (a). (C-F) mTDP-43 specificity of 15A by IHC. Sections of hippocampus (C-D) or cortex (E-F) from normal human (C, E) or nTg mouse brains (D, F) were stained with 15A, showing strong immunoreactivity for mouse neuronal nuclei, but no staining for human neuronal nuclei. Scale bar = 200 μm.

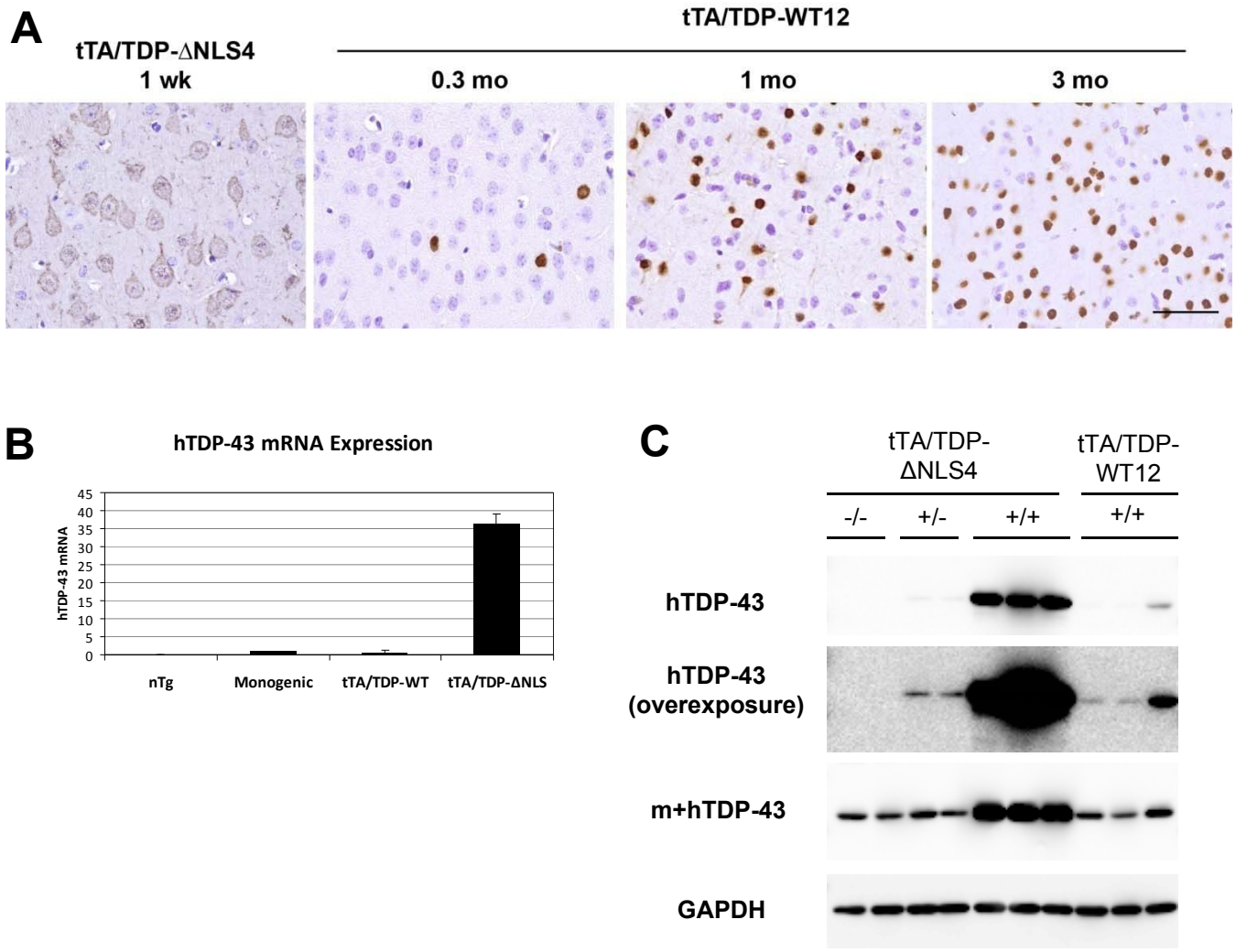

Figure S7. Low Expression of hTDP-43 in tTA/TDP-WT Mice 1-2 Weeks Off Dox. (A) IHC for hTDP-43 of neocortex shows early, uniform induction of transgene in tTA/TDP-ΔNLS4 mice and low numbers of hTDP-43 expressing neurons in tTA/TDP-WT12 mice at early timepoints off Dox. Scalebar = 50 μm. (B) qRT-PCR analysis using human specific TDP-43 primers showed low hTDP-43 mRNA levels in nTg, monogenic and tTA/TDP-WT mice in contrast to tTA/TDP-ΔNLS mice. Data shown as means +/- SEM of fold over control mice. (C) Immunoblot analysis of RIPA cortical lysates from mice analyzed in Fig 7 show low or undetectable hTDP-43 in nTg, monogenic and tTA/TDP-WT mice in contrast to tTA/TDP-ΔNLS mice.